Chapter 13
Laser-Stimulated Fluorescence Refines Flight Modeling of the Early Cretaceous Bird *Sapeornis*

FRANCISCO J. SERRANO,[1] MICHAEL PITTMAN,[2] THOMAS G. KAYE,[3] XIAOLI WANG,[4] XIAOTING ZHENG,[4] AND LUIS M. CHIAPPE[5]

ABSTRACT

Unseen and difficult-to-see soft tissues of fossil birds revealed by laser-stimulated fluorescence (LSF) shed light on their functional morphology. Here we study a well-preserved specimen of the early pygostylian *Sapeornis chaoyangensis* under LSF and use the newly observed soft-tissue data to refine previous modeling of its aerial performance and to test its proposed thermal soaring capabilities. Under LSF, the body's lateral outline is observed, permitting direct estimates of the body's disc surface that generates drag during flight (S_b). This surface and the body drag coefficient—which is better estimated knowing S_b— are influential parameters in modeling flight dynamics. In particular, we focus on two aspects of flight dynamics: the calculation of the power margin during flapping flight (power curve), and the sinking speed during gliding (glide polar). Results from revised models using our direct soft-tissue measurements support the notion that *Sapeornis* was a thermal soarer that glided for long periods. LSF also confirms the absence of a true alula in *Sapeornis*. While the deployment of the alular digit could have enhanced control during slow flight, the position of this digit along the handwing (distal part of the wing) suggests limited maneuverability. This study demonstrates how soft-tissue preservation can be incorporated into modeling of flight dynamics in light of ever-improving palaeontological imaging techniques.

INTRODUCTION

Laser-stimulated fluorescence (LSF) uses high flux laser light to fluoresce fossil specimens at macro- and microscopic scales, improving imaging results with respect to conventional UV light (Kaye et al., 2015). LSF has revealed otherwise obscure and invisible osteological and soft-tissue details in fossil specimens facilitating the reconstruction of a range of paleobiological aspects (Kaye et al., 2015, 2019a; 2019b; Falk et al., 2016a; Mayr et al., 2016; Vinther et al., 2016; Wang et al., 2017; Yang et al., 2018). LSF has helped improve our understanding of theropod flight evolution by directly revealing soft-tissue outlines of the wings and body, providing invaluable insights into the functional morphology of the first flyers including potential candidates (e.g., the early-diverging paravian *Anchiornis* (Wang et al., 2017) and the early pygostylian *Confuciusornis* (Falk et al., 2016b).

[1] Real Academia de Ciencias Exactas, Físicas y Naturales, Madrid; Dinosaur Institute, Natural History Museum of Los Angeles County, Los Angeles.
[2] Vertebrate Palaeontology Laboratory, Division of Earth and Planetary Science, the University of Hong Kong, Hong Kong.
[3] Foundation for Scientific Advancement, Sierra Vista, AZ.
[4] Institute of Geology and Paleontology, Linyi University, Linyi City, Shandong, China; Shandong Tianyu Museum of Nature, Pingyi, Shandong, China.
[5] Dinosaur Institute, Natural History Museum of Los Angeles County, Los Angeles

The flight dynamics of the Early Cretaceous early pygostylian *Sapeornis chaoyangensis* have been explored through quantitative approaches (Serrano and Chiappe, 2017). Morphofunctional evidence and aerodynamic models generated for this early bird indicated that *Sapeornis* flew by gliding over long periods and using ascending air currents in continental environments for soaring (i.e., thermal soaring). Serrano and Chiappe (2017) applied information from exquisitely preserved wing feathers to reconstruct the shape and size of the wings of this bird. Nonetheless, this approach was unable to include information from the body outline due to the absence of reliable nonfeather soft-tissue evidence from the studied specimens.

The body outline provides information about the body (= parasite) drag—the aerodynamic force generated by the body against the air stream—acting on a flying bird. As the generation of aerodynamic theoretical models is limited by a few parameters that are difficult to measure in flying birds (Pennycuick, 1969; Tucker, 1973; Rayner, 1999; Pennycuick, 2008), calculations for extinct birds require assumptions about such parameters (Burgers and Chiappe, 1999; Templin, 2000; Chatterjee and Templin, 2003; Ksepka, 2014; Serrano and Chiappe, 2017; Serrano et al., 2018). Among them, the body drag is particularly controversial and yet, it is proven to have a strong influence on the results of the models (Hedenström and Rosén, 2003; Taylor et al., 2016). LSF imaging of *Sapeornis* specimen STM 15-15 (Shandong Tianyu Museum of Nature, Pingyi, China) now provides information on body shape for the first time (fig. 1). Using this new soft-tissue information, we reanalyze the flight dynamics of this early pygostylian. We also provide a novel comparative analysis for the alular digit position of this bird, as this structure is very important for controlling flight at low speeds (Meseguer et al., 2012; Lee et al., 2015). Our refined results of the flight performance of this bird—incorporating both body drag and the role of the alular digit—allow us to test existing hypotheses about the flying habits and paleoecological inferences of *Sapeornis*.

MATERIAL AND METHODS

Fossil and Estimations

Sapeornis chaoyangensis STM 15-15 (fig. 1) was examined and photographed at the Shandong Tianyu Museum of Nature (Pingyi, China). Bone measurements (table 1) were taken from photographs using ImageJ 1.51j8 (available from http://imagej.nih.gov/ij). Body width (L_b) was measured from the LSF image as the maximum length from the dorsal margin of the vertebral column to the ventral contour of the feathered body (fig. 2). Despite the well-preserved feathers revealed by LSF, the wingtip (i.e., the distance between the distal end of the second phalanx of the major digit and the tip of the wing) and the wing chord (i.e., the distance from leading to trailing edge at wrist level) are not measurable for STM 15-15. Their values were obtained assuming an isometric variation for the skeletal wing (i.e., the added length of humerus, ulna, carpometacarpus, and major digit) of specimen DNHM 3078 (Gao et al., 2012). Following Serrano and Chiappe's (2017) study of the aerodynamics of *Sapeornis*, we estimated the body mass (M_b), wingspan (B), and lift surface (S_L) of STM 15-15 using multiple regressions derived from a dataset of modern flying birds (Serrano et al., 2015; Serrano et al., 2017).

Laser-Stimulated Fluorescence (LSF)

LSF images were collected using a refined version of the original protocol of Kaye et al. (2015) (Wang et al., 2017; Kaye et al. 2019a, 2019b). *Sapeornis* specimen STM 15-15 was imaged at the Shandong Tianyu Museum of Nature with a 405 nm violet laser. An appropriate long-pass blocking filter was used in front of a Nikon D810 DLSR camera lens to prevent image saturation by the laser. The laser was dispersed into a vertical line by a Laserline Optics

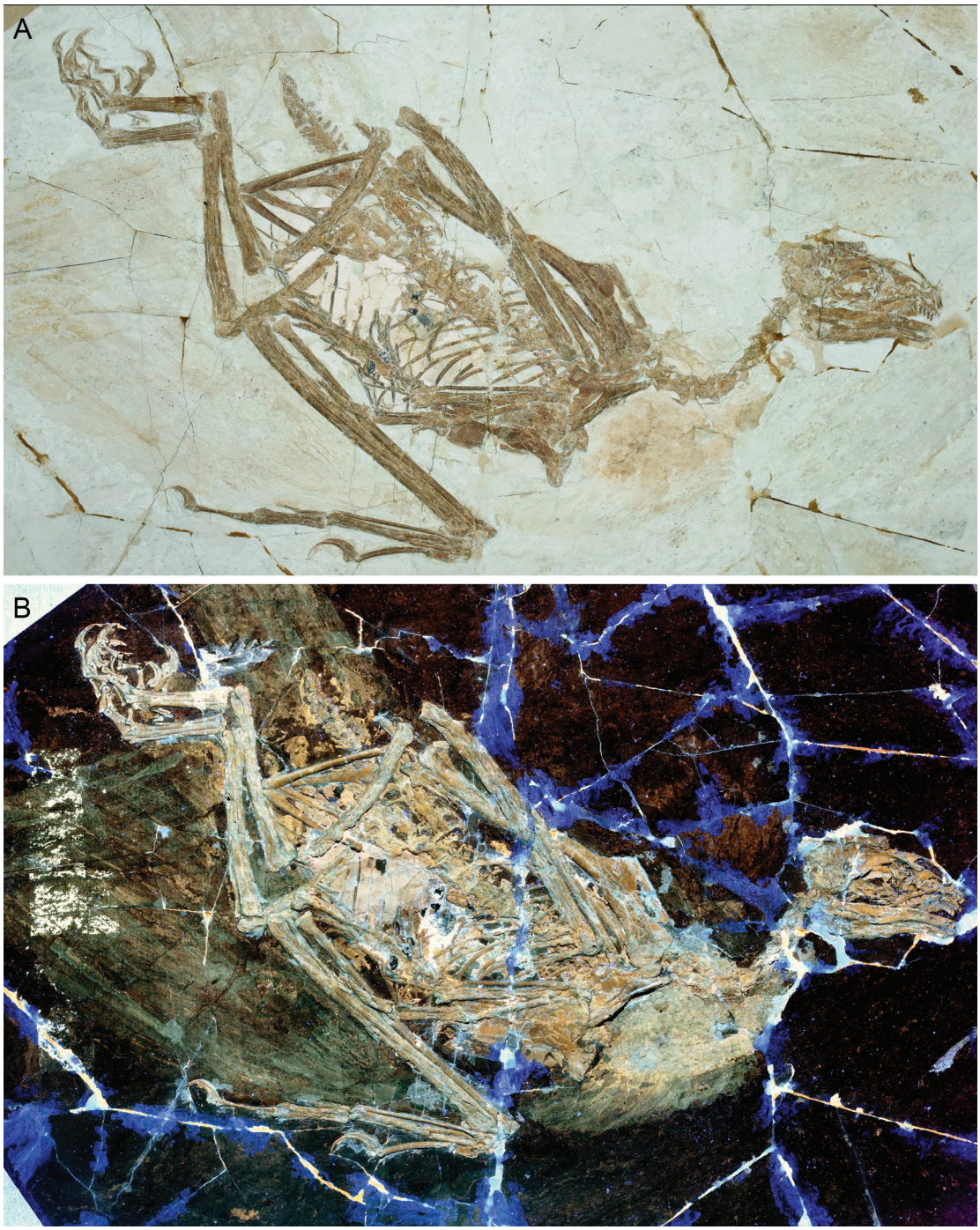

FIG. 1 Early pygostylian *Sapeornis* STM 15-15 shows faint soft-tissue details that **A,** under white light are vivid and **B,** under LSF, extensive.

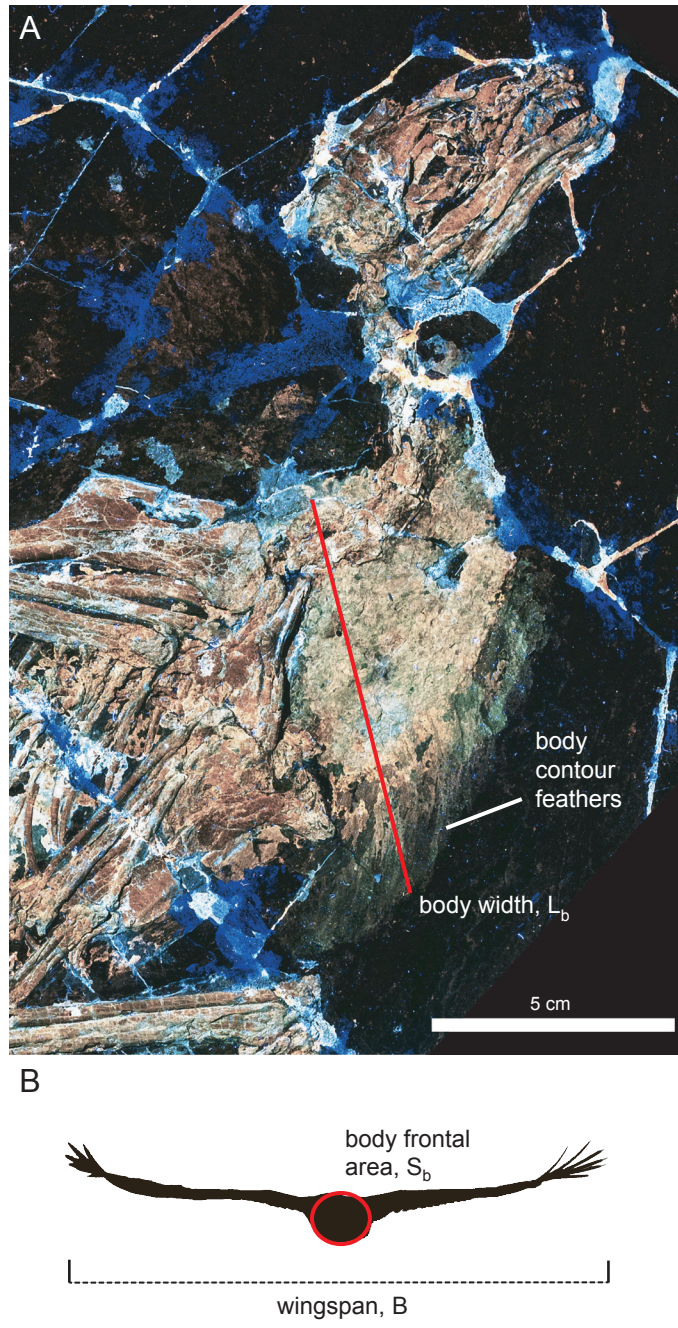

FIG. 2. **A.** The anterior region of *Sapeornis* STM 15-15 under LSF, showing contour feathers. **B.** Frontal view silhouette showing S_b and B.

Canada lens, which was mechanically swept repeatedly over the specimen during photo time exposures in the museum's dark room. The images were postprocessed in Photoshop CS6 for sharpness, color balance, and saturation. Details of the theory behind LSF imaging can be found in Wang et al. (2017).

Flight Dynamics Modeling

In modern birds, the maximum available power output (aerobic metabolism) for attaining active flight (P_{av}) scales negatively with body size (Templin, 2000; Pennycuick, 2008). P_{av} was calculated using an oxygen consumption rate (V_{O2}, mL/s) in which 1 mL O_2/s generates 20.1 W during aerobic activity (Schmidt-Nielsen, 1997). Values of V_{O2} were estimated for *Sapeornis* using Equation 1, which was derived from birds flying at modern O_2 concentration (i.e., 20.9 mL O_2/100 mL air; Bishop and Butler, 2015):

$$(1)\ V_{O2} = 160\ M_b^{\,0.74}$$

By assuming a conversion efficiency of 0.2 from the total metabolic power input to P_{av} (Tucker, 1973; 1975; Pennycuick, 2008), and translating minutes into seconds—as Equation 1 was derived from V_{O2} measured in mL/min—the P_{av} at modern conditions was calculated using Equation 2:

$$(2)\ P_{av} = 20.1 \times 0.2 / 60\ V_{O2}$$
$$P_{av} = 0.067\ V_{O2}$$

Values of P_{av} for STM 15-15 were adjusted to the O_2 atmospheric levels at 120 Myr, the estimated time of deposition for the fossil (Ward and Berner, 2011), through the percentage of variation between concentrations today and in the past (Serrano et al., 2019), calculated using Equation 3 (where AOC is atmospheric O_2 concentration):

$$(3)\ P_{av} = (0.067\ V_{O2} \cdot \%\Delta\ AOC) + 0.067\ V_{O2}$$

TABLE 1
Anatomical measurements (in mm) of *Sapeornis* STM 15-15
Asterisk indicates estimated measurements due to specimen damage or incomplete preservation.

Element	Measurement
Humerus	132.7
Humerus midshaft width	6.9
Distal humeral width	14.2
Deltopectoral crest	48
Bicipital crest	15.6
Ulna	129.5
Ulna midshaft width	7.0
Distal ulnar width	9.1
Radius	128.2
Radius midshaft width	3.5
Carpometacarpal length (semilunate to major metacarpal)	61.7
Alular digit position (semilunate to distal end of alular mc)	16.7
Proximal carpometacarpus width	11.1
Metacarpus midshaft width	6.5
Major metacarpal midshaft width	4.3
Alular digit	31.5
Major digit-1	30
Major digit-2	26.4
Wing tip*	225.8
Wing chord*	240.7
Femur	68.4
Femur midshaft width	5.9
Tibiotarsus	79.6
Metatarsal	43.6
Body width	95.7

For a given bird flying, the power curve that relates its forward speed (V_t) with its mechanical power output necessary for flapping flight (P_{mec}) is U-shaped (Pennycuick, 1969; Tucker, 1973; Rayner, 1999). This theoretical relationship is mostly supported by direct measure of the input power in modern birds flapping (Bishop and Butler, 2015). We constructed power curves for

Sapeornis STM 15-15 using the software Flight v. 1.24 (www.bio.bristol.ac.uk/people/pennycuick.htm) (Pennycuick, 2008). The values of P_{mec} for a range of velocities V_t were calculated according to Equation 4, as the summation of the induced power (P_{ind}; Equation 5, where k is the induced power factor and g is gravitational acceleration), the parasite power (P_{par}; Equation 6, where S_b is the frontal area of the body, C_{Db} is the body-drag coefficient, ρ_{air} is the density of air and B is the wingspan), and the profile power (P_{pro}; Equation 7, where V_{mp} is the minimum power speed and C_{pro} is the profile power constant).

(4) $P_{mec} = P_{ind} + P_{par} + P_{pro}$
(5) $P_{ind} = 2k\ [M_b\ g]^2\ /\ V_t\ \pi\ B^2 \rho_{air}$
(6) $P_{par} = \rho_{air}\ V_t^3\ S_b\ C_{Db}\ /\ 2$
(7) $P_{pro} = [2k\ (M_b\ g)^2\ /\ V_{mp}\ \pi\ B_2\ \rho_{air} + \rho_{air}\ V_{mp}{}^3 S_b\ C_{Db}\ /2]\ C_{pro}\ /[B_2/S_L]$

These calculations require assumptions for some components, particularly when applied to fossil taxa (Serrano et al., 2018). For example, k—a parameter that accounts for any deviations from elliptical distribution of the lift across the wingspan— was set at $k = 1.2$, a value typically observed in aircraft, while C_{pro} was fixed at 8.4 to make P_{pro} proportional to the wing area (Pennycuick, 2008). The body-drag components (i.e., S_b and C_{Db}) are highly influential parameters (Taylor et al., 2016), and they were addressed, as explained in the next section. The cruising speed or the speed with minimum cost of transport (V_{mr}), was calculated as the speed where the tangent to the power curve intersects with the origin of the speed-power plot (Rayner, 1999).

The dynamics of gliding were studied through the glide polar graph that relates the sinking speeds (V_z) to a range of forward speed (V_t). V_z calculated with Equation 8, where D is the total aerodynamic drag resulting from the addition of the induced, parasite and profile drags (Pennycuick 2008). We also assumed that wingspan decreases as a linear function of speed (i.e., linear reduction command of Flight v. 1.24) and used an induced drag factor equal to 1.0 (Taylor et al., 2016):

(8) $V_z = D\ V_t\ /\ M_b\ g$

Body-Drag Estimation

The body frontal area (S_b) of STM 15-15 was calculated directly (Equation 9) from the measurement of the body width (L_b; fig. 2). For comparison, S_b was also calculated from its allometric relationship with the body mass, M_b (Equation 10) (Pennycuick et al., 1988).

(9) $S_b = \pi\ *\ (L_b\ /\ 2)^2$
(10) $S_b = 0.00813\ *\ M_b{}^{0.666}$

The body-drag coefficient (C_{Db}) is a dimensionless value that indicates the streamlined degree of the body (Pennycuick, 2008). C_{Db} value is difficult to measure in modern birds, and we used different approaches for obtaining it in *Sapeornis*.

The first approach, named model 1, was based on the Reynold's number of the body (Re_b) (Equation 11). C_{Db} was calculated from its negative allometry with Re_b (Equation 12) found in 39 modern passerines (Hedenström and Liechti, 2001).

(11) $Re_b = V_t\ L_b\ \rho_{air}\ \mu^{-1}$
(12) $C_{Db} = 0.70 - (5.8 \times 10^{-6})\ Re_b$

We took the ρ_{air} at 120 Myr (i.e., 1.209 kgm^{-3}; Serrano et al., 2019), while the dynamic viscosity of the air, μ, was assumed at modern standard conditions (i.e., 1 atm, 20° C). Under this approach C_{Db} varies with Re_b, and this Re_b is dependent on Vt. We calculated Re_b and C_{Db} at each V_t, from 7 to 24 ms^{-1} (i.e., the range for plausible flight speed of *Sapeornis* given by Serrano and Chiappe 2017). The average value of these C_{Db} was used to construct the models.

Another approach, model 2, obtained C_{Db} from S_b (Eq. 10) and the equivalent flat-plate area (A) (Equation 13). For estimating A, we followed the approach from Taylor and Thomas (2014) that assumes a body drag equivalent to the drag on a flat plate with 1% of the area of the wings (Equation 14). Rearranging equations 13 and 14, C_{Db} was estimated in Equation 15.

(13) $A = S_b \times C_{Db}$
(14) $A = 0.01\ S_L$
(15) $C_{Db} = (0.01\ S_L) / S_b$

Lastly, we generated models with minimum and maximum C_{Db} values (models 3 and 4, respectively) to obtain an uncertainty range for the curves. The minimum C_{Db} was fixed at 0.1, a value that assumes a well-streamlined body with no drag generated from the legs and feet (Pennycuick, 2008). We selected the maximum C_{Db} at 0.5 because Hedenström and Liechti (2001) suggested that C_{Db} experimentally measured above 0.4 would come from the underestimation of the maximum effort of the flying birds tested, although they found outliers above 0.5. Models 3 and 4 used S_b from Equation 10.

RESULTS

For *Sapeornis* STM 15-15 we estimated a M_b of 0.927 kg, a B of 122.3 cm and S_L of 0.235 m^2, within the range provided by Serrano and Chiappe (2017). From its M_b, STM 15-15 could generate a maximum P_{av} of 9.0 W. C_{Db} values calculated from Re_b (model 1: $C_{Db} = 0.31$) and from A (model 2: $C_{Db} = 0.30$) are within the range established between the minimum and maximum values (i.e., 0.1 and 0.5 in the models 3 and 4, respectively). The three power curves (models 1, 2, and 4) show that the P_{mec} required for sustaining flapping flight was above the value of P_{av} for the full range of V_t (fig. 3A). In model 3—the one assuming the minimum C_{Db}—the P_{mec} was slightly under P_{av} at starting values of the V_t range. At cruising speeds V_{mr}, all models show that P_{mec} was higher than the P_{av}. The four aerodynamic models thus indicate that STM 15-15 could not generate sufficient P_{mec} for sustaining a prolonged flight through wing flapping.

The glide polar graph illustrates that in STM 15-15 sinking took place at low forward speeds (fig. 3B). This gliding pattern, observed in the four analyzed models (1, 2, 3, and 4), has values within the range of modern birds that use thermal soaring. Model 1—the one using direct information from the fossil's body outline—clearly shows a glide pattern like a thermal soarer; when STM-15-15 reached its maximum lift-to-drag ratio (11.8-12.1), its gliding-forward velocity was 9.7 ms^{-1} (9.2–10.1 ms^{-1}) and its sinking speed 0.82 ms^{-1} (0.76–0.86 ms^{-1}). These values are remarkably close to those for the Red-Tailed Hawk (*Buteo jamaicensis*), as reported in Serrano and Chiappe (2017: table 2).

The position of the alular digit in STM 15-15 (fig. 4)—here based on the location of the distal end of the alular metacarpal—is farther from the wrist than that observed in similar-sized soaring birds (fig. 5). Such a distalward position resembles modern birds that are poorly competent at unsteady maneuvers, typically divers (i.e., loons, grebes, auks, diving ducks, cormorants, and storm petrels) or occasional fliers (i.e., landfowls, waterfowls, and rails). Pelicans and South American screamers, more than double the size of STM 15-15, were the only thermal soarers with a comparable distalward position of the alular digit (fig. 5).

DISCUSSION

Our study is the first to use the preserved body outline of a fossil bird—as revealed under LSF (fig. 2B)—to refine its flight modeling. Visualization of the body outline of STM 15-15 allows a direct measure of the body surface that generated drag during flight (L_b and S_b) (i.e., model 1), whereas previous aerial models of *Sapeornis* (Serrano and Chiappe, 2017) assumed a modern allometric variation for S_b (Pennycuick et al., 1988) (i.e., models 2, 3 and 4). Visualization of the body outline also allows a direct calculation of the body-drag coefficient (C_{Db}), which has proven especially controversial to calculate from theoretical approaches (Taylor et al., 2016). Our results show that C_{Db} value calculated in model 1—direct calculation through the Reynolds number of the body (Hedenström and Liechti, 2001)—was similar to the value calculated in model 2, a calculation that assumed a body-drag equivalent to the drag on a flat plate with 1% of

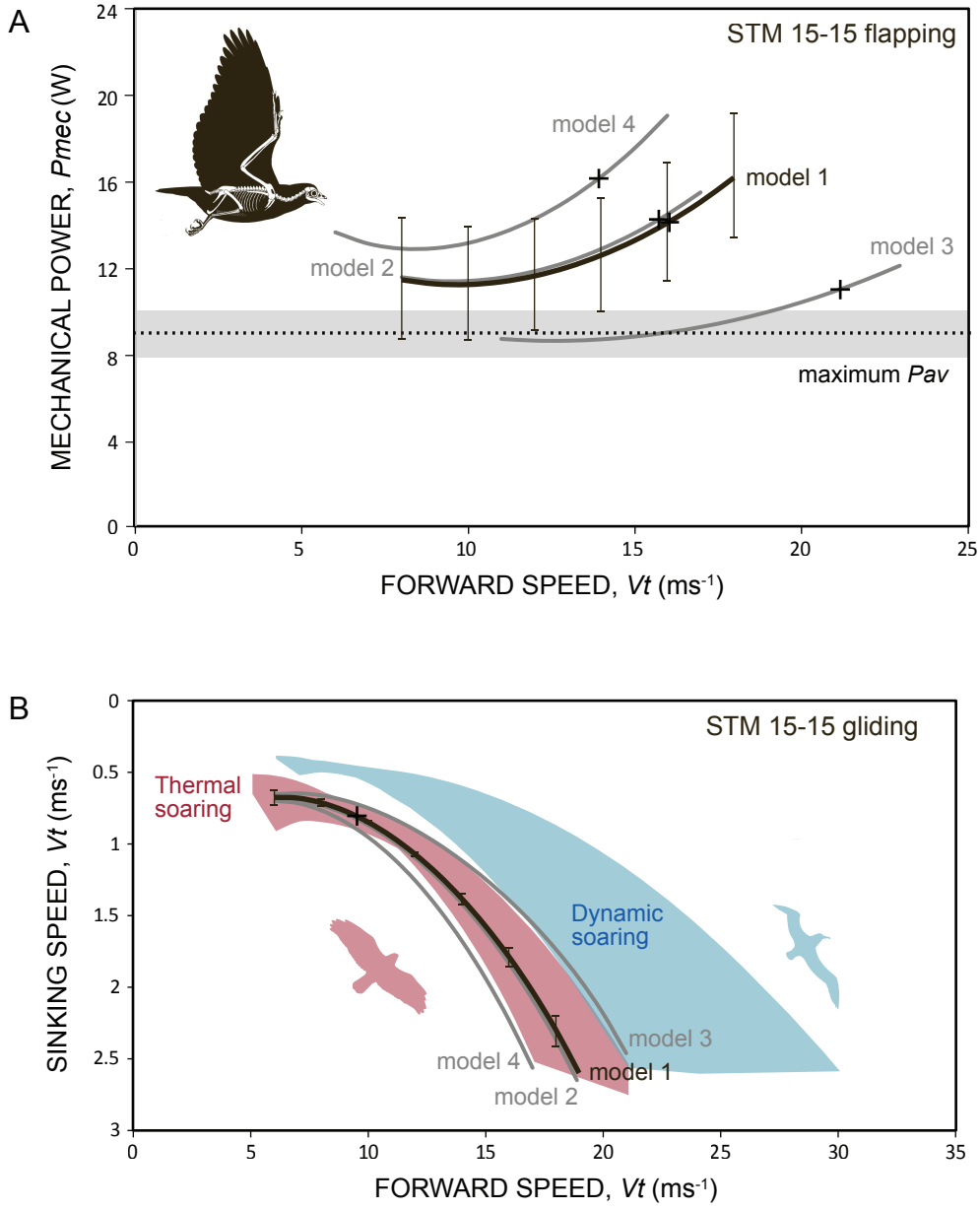

FIG. 3. **A.** Power margin in four models of *Sapeornis* STM 15-15. **B.** Glide polar graph in 4 models of STM 15-15 compared to modern soaring birds.

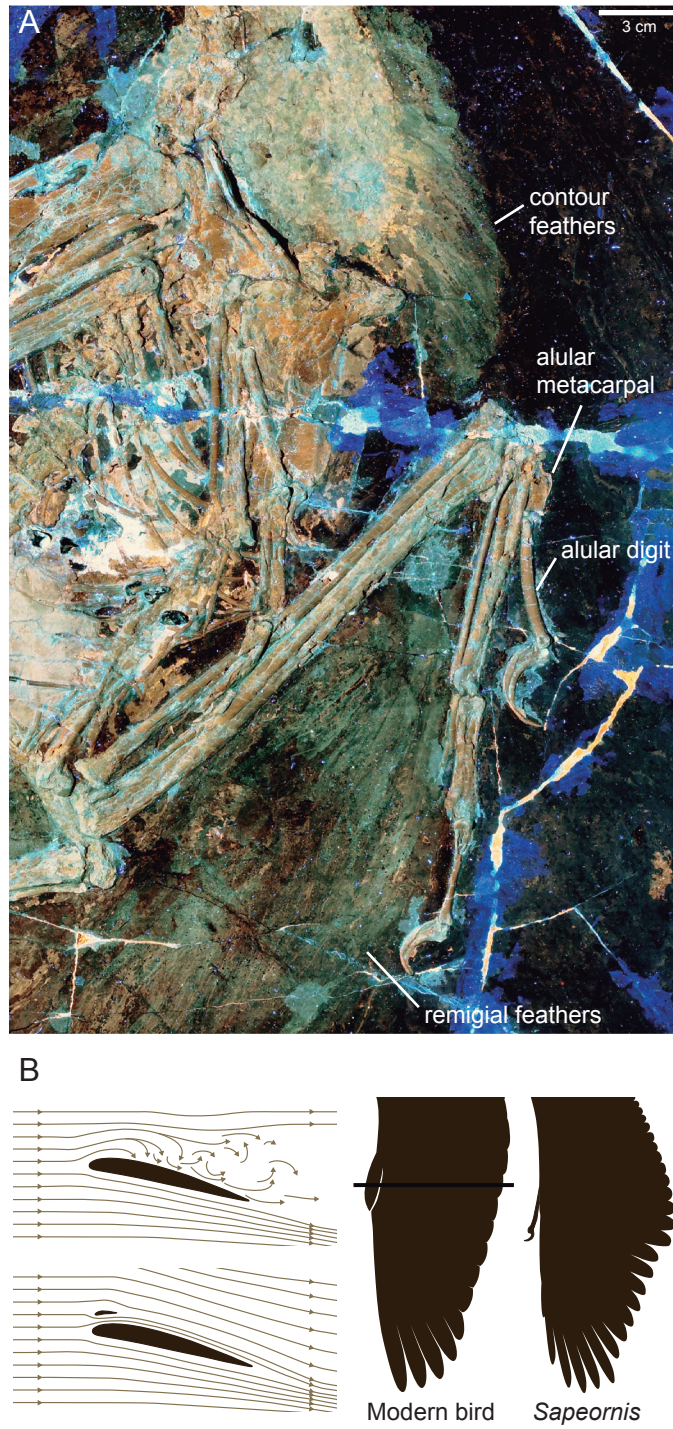

FIG. 4. **A.** LSF image of hand and feathers of STM 15-15. **B.** Effect of alula delaying stall, and wing silhouettes of an avian (crown bird) and *Sapeornis*.

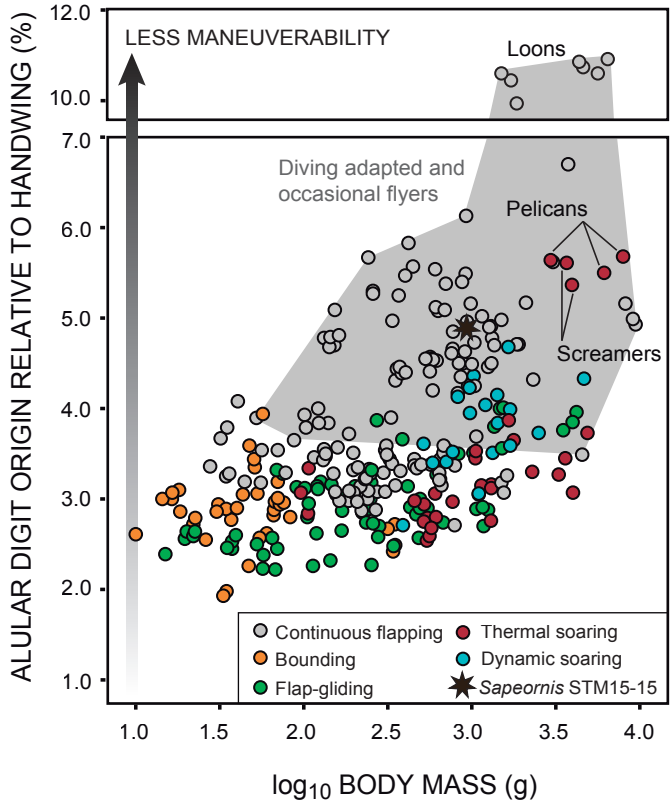

FIG. 5. Scatter graph of alular digit position against M_b, compared with modern bird morphospace.

the area of the wings (Taylor and Thomas, 2014). The congruence between the aerodynamic models 1 and 2 (fig. 3) validates the assumptions made in Serrano and Chiappe's (2017) previous assessment of the flight performance of *Sapeornis*. However, such assumptions should probably be validated on a case-by-case basis, especially given the often large morphological differences between modern and early-diverging bird species as well as the availability of direct soft-tissue data using imaging methods like LSF. In order to minimize this issue, we delimited the flight reconstruction of STM 15-15 using minimum and maximum values (models 3 and 4) based on C_{Db} observed in modern birds (Pennycuick, 2008; Hedenström and Liechti, 2001). Finally, the negative power margin during flapping flight and the gliding pattern obtained in the four models (fig. 3) corroborate the hypothesis that *Sapeornis* had thermal soaring capabilities, as proposed by Serrano and Chiappe (2017).

Furthermore, we argue that the alular digit, albeit lacking a true alula as shown by LSF (fig. 4A), was a functional precursor of the true alula (Meseguer et al., 2012), thus acting as an anti-stall device that increased control at low speeds (fig. 4B). Our study documents a distalward location of the alular digit of *Sapeornis* (fig. 5), which implies that a lesser portion of the proximal handwing was under the influence of this flap. Such position of the alular digit (and functional flap) suggests that the maneuverability of *Sapeornis* might have been weak when compared with that of modern soaring birds of similar size. Lastly, from a paleoecological perspective, these results indicate that if *Sapeornis* was capable of perching, as suggested by the bird's pedal anatomy (Glen and Bennett, 2007;

Chiappe and Meng, 2016), its limited capacity to maneuver would have hindered its abilities to land on a perch.

ACKNOWLEDGMENTS

We would like to thank Kenneth H.C. Fung and First Initiative Foundation for their support of the International Pennaraptoran Dinosaur Symposium, the venue where we got the idea for this study. This project was supported by the Seed Fund for Basic Research for Resubmission of GRF/ECS Proposals from the University of Hong Kong (to M.P.) and funding from the HKU MOOC course Dinosaur Ecosystems (to M.P.). F.J.S. was supported by a Juan de la Cierva – Incorporación Postdoctoral Fellowship and the Research Project CGL2016-78577-P funded by the Spanish Ministry of Economy, Industry and Competitiveness. X.L.W. was supported by the Taishan Scholars Program of Shandong Province (No. Ts20190954). We would like to dedicate this chapter to the memory of C.J. Pennycuik.

REFERENCES

Bishop, C.M., and P.J. Butler. 2015. Flight. *In* C.G. Scanes (editor), Sturkie's Avian Physiology: 919–974. London: Academic Press

Burgers, P., and L.M. Chiappe. 1999. The wing of *Archaeopteryx* as a primary thrust generator. Nature 399: 60–62.

Chatterjee, S., and R.J. Templin. 2003. The flight of *Archaeopteryx*. Naturwissenschaften 90: 27-32.

Chiappe, L.M., and Q. Meng. 2016. Birds of stone. Baltimore: Johns Hopkins University Press.

Falk, A.R., T.G. Kaye, Z.H. Zhou, and D.A. Burnham. 2016a. Laser fluorescence illuminates soft tissues and life habits of *Confuciusornis*. PLoS One: undergoing postreview corrections.

Falk, A.R., T.G. Kaye, Z.H. Zhou, and D.A. Burnham. 2016b. Laser fluorescence illuminates the soft tissue and life habits of the Early Cretaceous bird *Confuciusornis*. PLoS One 11: e0167284.

Gao, C., et al. 2012. A subadult specimen of the Early Cretaceous bird *Sapeornis chaoyangensis* and a taxonomic reassessment of sapeornithids. Journal of Vertebrate Paleontology 32: 1103–1112.

Glen, C.L., and M.B. Bennett. 2007. Foraging modes of Mesozoic birds and non-avian theropods. Current Biology 17: R911–R912.

Hedenström, A., and F. Liechti. 2001. Field estimates of body drag coefficient on the basis of dives in passerine birds. Journal of Experimental Biology 204: 1167–1175.

Hedenström, A., and M. Rosén. 2003. Body frontal area in passerine birds. Journal of Avian Biology 34: 159–162.

Kaye, T.G., et al. 2015. Laser-stimulated fluorescence in paleontology. PLoS One 10: e0125923.

Kaye, T.G., M. Pittman, G. Mayr, D. Schwarz, and X. Xu. 2019a. Detection of lost calamus challenges identity of isolated *Archaeopteryx* feather. Scientific Reports 9: 1182.

Kaye, T.G., et al. 2019b. Fully fledged enantiornithine hatchling revealed by Laser-Stimulated Fluorescence supports precocial nesting behavior. Scientific Reports 9: 5006.

Ksepka, D.T. 2014. Flight performance of the largest volant bird. Proceedings of the National Academy of Sciences of the United States of America 111: 10624–10629.

Lee, S., J. Kim, H. Park, P.G. Jabłoński, and H. Choi. 2020. The function of the alula in avian flight. Scientific Reports 5: 9914.

Mayr, G., M. Pittman, E. Saitta, T.G. Kaye, and J. Vinther. 2016. Structure and homology of *Psittacosaurus* tail bristles. Palaeontology 59: 793–802.

Meseguer, J., et al. 2012. Lift devices in the flight of *Archaeopteryx*. Spanish Journal of Paleontology 27: 125–130.

Pennycuick, C.J. 1969. The mechanics of bird migration. Ibis 111: 525–556.

Pennycuick, C.J. 2008. Modelling the flying bird. London: Academic Press.

Pennycuick, C.J., H.H. Obrecht, and M.R. Fuller. 1988. Empirical estimates of body drag of large waterfowl and raptors. Journal of Experimental Biology 135: 253–264.

Rayner, J.M. 1999. Estimating power curves of flying vertebrates. Journal of Experimental Biology 202: 3449–3461.

Schmidt-Nielsen, K. 1997. Animal physiology: adaptation and environment. Cambridge: Cambridge University Press.

Serrano, F.J., and L.M. Chiappe. 2017. Aerodynamic modelling of a Cretaceous bird reveals thermal soaring during avian evolution. Journal of the Royal Society Interface 14: 20170182.

Serrano, F.J., P. Palmqvist, and J.L. Sanz. 2015. Multivariate analysis of neognath skeletal measurements: implications for bodymass estimation in Mesozoic birds. Zoological Journal of the Linnean Society 173: 929–955.

Serrano, F.J., P. Palmqvist, L.M. Chiappe, and J.L. Sanz. 2017. Inferring flight parameters of Mesozoic avians through multivariate analyses of forelimb elements in their living relatives. Palaeobiology 43: 144–169.

Serrano, F.J., et al. 2018. Flight reconstruction of two European enantiornithines (Aves, Pygostylia) and the achievement of bounding flight in Early Cretaceous birds. Palaeontology 61: 359–368.

Serrano, F.J., et al. 2019. The effect of long-term atmospheric changes on the macroevolution of birds. Gondwana Research 65: 86–96.

Taylor, G.K., K.V. Reynolds, and A.L. Thomas. 2016. Soaring energetics and glide performance in a moving atmosphere. Philosophical Transactions of the Royal Society of London Series B Biological Sciences 371: 20150398.

Templin, R.J. 2000. The spectrum of animal flight: insects to pterosaurs. Progress in Aerospace Science 36: 393–436

Tucker, V.A. 1973. Bird metabolism during flight: evaluation of a theory. Journal of Experimental Biology 58: 689–709.

Tucker, V.A. 1975. The energetic cost of moving about: walking and running are extremely inefficient forms of locomotion. Much greater efficiency is achieved by birds, fish—and bicyclists. American Scientist 63: 413–419.

Vinther, J., et al. 2016. 3D camouflage in an ornithischian dinosaur. Current Biology 26: P2456–2462.

Wang, X.L., et al. 2017. Basal paravian functional anatomy illuminated by high-detail body outline. Nature Communications 8: 14576.

Ward, P., and R. Berner. 2011. Why were there dinosaurs? Why are there birds? *In* G. Dyke and G. Kaiser (editors), Living dinosaurs: the evolutionary history of modern birds: 30–38. Oxford: Wiley-Blackwell.

Yang, Z.X., et al. 2018. Pterosaur integumentary structures with complex feather-like branching. Nature Ecology and Evolution 3: 24–30.